Ionics (2023) 29:675–683
https://doi.org/10.1007/s11581-022-04824-9

ORIGINAL PAPER

In situ preparation of $Ni(OH)_2/CoNi_2S_4$/NF composite as efficient electrocatalyst for hydrogen evolution reaction

Yanxia Wu[1] · Lirong Su[1] · Qingtao Wang[1] · Shufang Ren[2]

Received: 19 August 2022 / Revised: 7 October 2022 / Accepted: 13 November 2022 / Published online: 1 December 2022

Abstract

It is an effective strategy to improve the catalytic activity of materials by constructing hydroxide/sulfide hybrid structure. In this work, nickel hydroxide/CoNi sulfide ($Ni(OH)_2/CoNi_2S_4$) nanoflowers supported on nickel foam (NF) were synthesized by simple hydrothermal reaction and subsequent sulfurization, used as an efficient hydrogen evolution reaction (HER) electrocatalyst in acidic medium. The results show that as-synthesized $Ni(OH)_2/CoNi_2S_4$/NF catalyst exhibits good HER catalytic activity and stability in acidic electrolyte. When the current density is 10 mA cm^{-2}, the overpotential and Tafel slope of $Ni(OH)_2/CoNi_2S_4$/NF in 0.5 M H_2SO_4 solution is 124 mV and 84 mV dec^{-1}, respectively, displaying better catalytic activity than $Ni(OH)_2$/NiS/NF. The introduction of Co and synergistic effect of Co and Ni bimetallic sites promote the HER activity of the catalyst. In addition, the unique nanoflower structure of $Ni(OH)_2/CoNi_2S_4$/NF catalyst increases the active area of the material, thus providing more catalytic active sites.

Keywords Transition metal sulfides · Electrocatalyst · Hydrogen evolution reaction · Electrolysis of water

Introduction

With the rapid development of modern industrial technology, the traditional fossil energy has been unable to meet the increasing demand of people [1, 2]. Long-term dependence on non-renewable fossil fuels will not only accelerate energy crisis but also cause many problems such as global warming and environmental pollution. Therefore, it is urgent to find an environmentally friendly, efficient, and renewable alternative energy [3, 4]. Hydrogen energy is considered as one of the ideal clean energies to replace fossil fuels because of its high energy density, environmental friendliness, and zero carbon emissions [5]. At present, hydrogen production technology via electrochemical water splitting is the most promising way to achieve sustainable development of energy and zero carbon emissions [6–8]. Electrolysis of water is composed of cathodic hydrogen evolution reaction (HER) and anodic oxygen evolution reaction (OER). However, slower kinetics and higher overpotential in the process of water splitting will seriously affect the efficiency of hydrogen production. The design and development of efficient and stable electrocatalysts can effectively reduce the overpotential in HER and improve the efficiency of hydrogen production [6]. At present, noble metal platinum-based (Pt) catalysts exhibit excellent HER catalytic activity, but their scarce reserves and high price limit the large-scale industrial applications [9]. So, it is urgent to develop non-noble metal-based catalysts with abundant reserves, low cost, high efficiency, and stability, which is very important for industrial application of electrolysis of water [10–12].

In recent years, the most studied non-noble metal HER catalysts are transition metal compounds, such as transition metal oxides/hydroxides [13, 14], borides [15, 16], carbides [17, 18], nitrides [19], phosphides [20], sulfides [21], and selenides [22]. Especially, transition metal sulfides (TMSs) have been widely studied as HER electrocatalysts because of their abundant defect sites, controllable electronic structure, and various forms [23, 24]. KIM et al. [25] prepared CoS_2 on

✉ Yanxia Wu
wuyx2014@nwnu.edu.cn

✉ Qingtao Wang
wangqt@nwnu.edu.cn

[1] Key Laboratory of Eco-Functional Polymer Materials of the Ministry of Education, College of Chemistry and Chemical Engineering, Instrumental Analysis Center, Northwest Normal University, Lanzhou 730070, China

[2] Key Laboratory of Evidence Science Research and Application of Gansu Province, Gansu University of Political Science and Law, Lanzhou 730070, China

carbon fiber paper (CFP), used as an efficient HER electrocatalyst, which exhibited high catalytic activity and stability because of its unique nanostructure and synergy with carbon substrate. ZELEKE et al. [26] synthesized a monolayer molybdenum disulfide (MoS_2) electrocatalyst on carbonized polyacrylonitrile, displaying excellent electrochemical HER performance. Many studies have confirmed that bimetallic sulfides show better catalytic performance than monometallic sulfides due to the fact that different chemical activity of bimetallic sulfides components leads to more defects, which is beneficial to providing more active sites. At the same time, the synergistic effect of bimetallic sites can effectively adjust the electronic structure, thus improving electrocatalytic activity [27]. Therefore, it is an effective strategy to improve the catalytic activity by constructing bimetallic sulfides with abundant active sites. WU et al. [28] successfully prepared Mn-doped molybdenum disulfide/reduced graphene oxide (Mn-MoS_2/rGO) composites by hydrothermal method. The results showed that as-prepared Mn-MoS_2/rGO exhibited better catalytic activity than undoped MoS_2/rGO. ZHANG et al. [29] synthesized bimetallic FeS/NiS/NF material by solvothermal sulfidation. Compared with monometallic FeS/NF and NiS/NF materials, FeS/NiS/NF showed better HER performance.

Some studies have also shown that the catalytic activity of the TMSs can be further improved by combining with other active substances, such as layered double hydroxides (LDHs). LDH shows better activity and stability because of its unique structure, but its poor electrical conductivity will limit its electrocatalytic activity. Therefore, it inspires us to combine LDH with TMSs to achieve hydroxide/sulfide hybrid structure. Because the high electrical conductivity of TMSs and high intrinsic activity of LDH can function simultaneously to compensate each other's drawbacks, which may improve the catalytic performance by taking advantage of the strong synergistic effects between different components [30–33]. WANG et al. [30] synthesized $CoNi_2S_4$@NiMn-LDH/SCC heterostructure nanoarrays on superhydrophilic carbon cloth, displaying high catalytic activity and stability as bifunctional electrocatalysts. WU et al. [34] prepared self-supporting hollow $Co(OH)_2$/Ni-Co-S nanotube arrays by hydrothermal method and subsequent sulfurization. The catalyst showed good electrocatalytic performance for OER, HER, and overall water splitting.

In addition, it is a promising strategy by in situ growth of active materials on binder-free three-dimensional (3D) conductive substrates such as NF, which is beneficial to heighten the conductivity, increase active surface area, promote electron transportation, and improve the catalytic activity of the materials [35–37]. Du et al. [38] constructed $Ni(OH)_2/Ni_3S_2$ heterojunction nanosheets on NF substrate, used as efficient electrocatalyst for OER and HER. $Ni(OH)_2/Ni_3S_2$/NF with unique nanostructure and high specific surface area showed better catalytic activity of OER and HER. CHEN et al. [37] reported that Fe, Rh-codoped Ni_2P nanosheet arrays were in situ grown on 3D NF under hydrothermal condition and successive phosphorization. As-synthesized Fe, Rh-Ni_2P/NF catalyst exhibited better electrocatalytic performances for the HER, OER, and overall water splitting. ZHANG et al. [39] prepared straw-like phosphorus-doped Co_2MnO_4 nanoneedle arrays supported on NF (P-Co_2MnO_4/NF) by successive hydrothermal treatment, oxidation, and P doping for high-efficiency HER.

In view of this, we constructed nickel hydroxide/CoNi bimetallic sulfide ($Ni(OH)_2/CoNi_2S_4$) nanoflower composite supported on NF substrate by simple hydrothermal reaction and subsequent sulfurization. As-synthesized $Ni(OH)_2/CoNi_2S_4$/NF exhibits good HER catalytic activity and stability in acidic medium and is used as an efficient HER electrocatalyst.

Experimental section

Materials

Hydrochloric acid, acetone, ethanol, and urea were produced from Sinopharm Chemical Reagent Co., Ltd. Nickel nitrate hexahydrate and cobalt nitrate hexahydrate were purchased from Shanghai Zhongqin Chemical Reagent Co., Ltd. Sodium sulfide nonahydrate and ammonium fluoride were supplied by Yantai Shuangshuang Chemical Co., Ltd. All chemicals utilized were of analytical grade and were used as supplied without any further purification.

Synthesis of $Ni(OH)_2/CoNi_2S_4$/NF

Nickel nitrate hexahydrate (2 mmol), cobalt nitrate hexahydrate (1 mmol), ammonium fluoride (6 mmol), and urea (10 mmol) were added to 20 mL of deionized water, forming a pink clarifying solution after stirring for 30 min. The above solution and acid-washed NF were introduced into 50 mL of high-pressure reactor and kept at 120 °C for 12 h in the oven. Bimetallic CoNi hydroxide (CoNi LDHs@NF) precursor supported on NF were prepared by simple hydrothermal reaction. Subsequently, the precursor was sulfurized at low temperature to produce $Ni(OH)_2/CoNi_2S_4$/NF. The obtained precursor and 20 mL of sodium sulfide nonahydrate solution were placed into 50 mL of high-pressure reactor and kept at 120 °C for 4 h in the oven. The product was naturally cooled down to room temperature, washed with ethanol and deionized water alternately for several times, and dried in a vacuum oven at 60 °C to obtain $Ni(OH)_2/CoNi_2S_4$/NF composite. It is a promising strategy by in situ growth of $Ni(OH)_2/CoNi_2S_4$ on binder-free 3D NF. The preparation process of $Ni(OH)_2/CoNi_2S_4$/NF is shown in Fig. 1. In

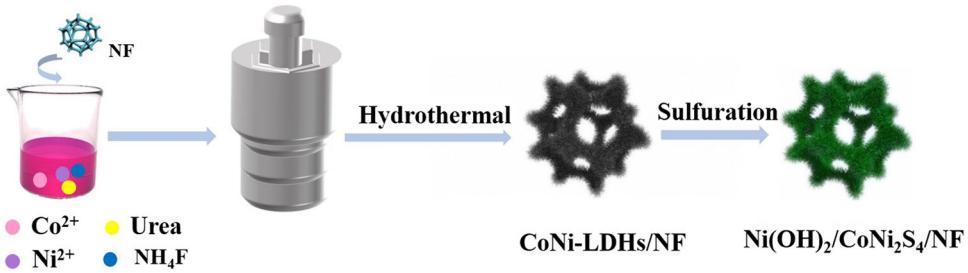

Fig. 1 Schematic illustration of the preparation of $Ni(OH)_2$/$CoNi_2S_4$/NF

addition, $Ni(OH)_2$/NiS/NF and $Ni(OH)_2$/NF were synthesized by the similar method, and their preparation process are given in the "Supplementary information."

Material characterization

X-ray diffraction (XRD) tests were performed on a D/Max-2400 powder diffractometer to analyze crystal phases of the as-synthesized materials. Scanning electron microscopy (SEM, JSM-6701F) was used to characterize the morphology of the materials. Transmission electron microscopy (TEM) and energy-dispersive X-ray (EDX) spectrometry measurements were carried out on a TF20 to characterize lattice fringes and chemical elements. X-ray photoelectron spectroscopy (XPS) characterization was performed on a PHI 5702 XPS instrument to analyze the chemical compositions and valence states of the materials.

Electrochemical measurements

All the electrochemical measurements were conducted on a three-electrode electrochemical cell by Autolab PGSTAT128N electrochemical workstation. $Ni(OH)_2$/$CoNi_2S_4$/NF and other samples as controls were used as the working electrode, Ag/AgCl as the reference electrodes, and graphite rod as counter electrode. Electrochemical tests were performed in 0.5 M H_2SO_4 electrolyte. The presented potentials in this work were all converted to reversible hydrogen electrode (RHE) via the equation: E (RHE) = E (Ag/AgCl) + 0.059 pH + 0.197. All of the polarization curves were recorded using linear sweep voltammetry (LSV). Electrochemical impedance spectroscopy (EIS) measurements were performed at the corresponding open circuit potential to the electrode with the frequency range of 50 kHz–0.01 Hz. The charge-transfer resistance (R_{ct}) was calculated by the diameter of the semicircular arc in the Nyquist plots. The double-layer capacitance (C_{dl}) values were determined by performing cyclic voltammetry (CV) measurements at different scanning rates of 20 ~ 100 mV s^{-1} under a non-Faradaic potential range.

Results and discussion

XRD tests were used to identify the crystal structure of materials. Figure 2 shows XRD patterns of the as-synthesized $Ni(OH)_2$/$CoNi_2S_4$ and $Ni(OH)_2$/NiS. From Fig. 2a, it can be seen that the diffraction peaks of $Ni(OH)_2$/$CoNi_2S_4$ are well indexed to $Ni(OH)_2$ (PDF#14–0117) and $CoNi_2S_4$ (PDF#24–0334). The peaks at 19.2, 33.0, 38.5, 52.1, 59.0, and 62.7° are assigned to (001), (100), (101), (102), (110), and (111) crystal planes of $Ni(OH)_2$ (PDF#14–0117), respectively. The diffraction peaks appeared at 16.2, 26.6, 31.4, 38.1, 50.2, and 55.0° are corresponding to (111), (220), (311), (400), (511), and (440) crystal planes of $CoNi_2S_4$ (PDF#24–0334), respectively. It indicates that $Ni(OH)_2$/$CoNi_2S_4$ composite was successfully prepared by hydrothermal reaction and subsequent sulfurization.

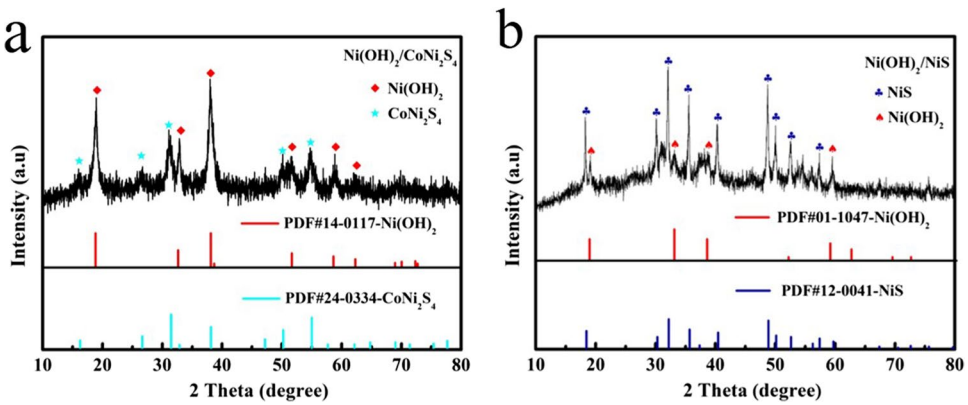

Fig. 2 XRD patterns of **a** $Ni(OH)_2$/$CoNi_2S_4$ and **b** $Ni(OH)_2$/NiS

Figure 2b presents XRD pattern of $Ni(OH)_2$/NiS. The diffraction peaks of $Ni(OH)_2$/NiS are also well indexed to $Ni(OH)_2$ (PDF#01–1047) and NiS (PDF#12–0041), demonstrating that $Ni(OH)_2$/NiS material was successfully synthesized. The XRD patterns of $Ni(OH)_2$ and CoNi LDHs are given in the "Supplementary information" (Fig. S1), and their diffraction peaks are basically consistent with the standard card.

Figure 3a–b shows the SEM images of $Ni(OH)_2$/NiS/NF. It can be clearly observed that a large number of $Ni(OH)_2$/NiS nanosheets were vertically grown on the surface of nickel foam. The porous structures formed by the interlaced nanosheets are beneficial to the ion migration of electrolytes and the release of bubbles produced by electrolysis of water. Figure 3c–d displays SEM images of $Ni(OH)_2/CoNi_2S_4$/NF. $Ni(OH)_2/CoNi_2S_4$/NF is characterized with nanoflowers composed of nanowire arrays and nanosheets. Furthermore, many nanowire arrays were grown on the surface of nanosheets. The unique structure of $Ni(OH)_2/CoNi_2S_4$/NF is helpful to increase specific surface area, expose more catalytic active sites, and improve the electrocatalytic performance of the material. As seen from TEM image of $Ni(OH)_2/CoNi_2S_4$ (Fig. 3e), as-prepared material exhibits nanoflowers structure composed of nanowire arrays and nanosheets, in agreement with the results of its SEM image in Fig. 3c–d. The high-resolution TEM image in Fig. 3f shows that the lattice fringes with distances of 0.233 and 0.283 nm correspond to (101) plane of $Ni(OH)_2$ (PDF#14–0117) and (311) plane of $CoNi_2S_4$ (PDF#24–0334), respectively. It demonstrates that as-prepared $Ni(OH)_2/CoNi_2S_4$ composite is composed of $Ni(OH)_2$ and $CoNi_2S_4$, which is consistent with its XRD results (Fig. 2a). The element composition and distribution of the material were analyzed by the EDX attached to TEM instrument. As shown in Fig. 3g–k, $Ni(OH)_2/CoNi_2S_4$ is mainly composed of Co, Ni, S, and O elements.

Because the surface structure and composition of the catalysts affect their catalytic activity, XPS is usually used to analyze the valence and surface chemical composition of the materials. Figure 4 displays the XPS spectrum of $Ni(OH)_2/CoNi_2S_4$/NF. The XPS survey spectrum of $Ni(OH)_2/CoNi_2S_4$/NF shows the presence of Ni, Co, S, and O elements in the material (Fig. 4a), which is basically consistent with the results of EDX. From the Ni 2p spectrum in Fig. 4b, two peaks located at 855.97 and 873.81 eV are ascribed to Ni $2p_{3/2}$ and Ni $2p_{1/2}$ of Ni^{2+} species, and the two peaks appeared at 861.97 and 880.08 eV correspond to the satellite peak of Ni^{2+} species [40–43]. The Co 2p spectrum in Fig. 4c shows that two peaks at 782.45 and 797.73 eV

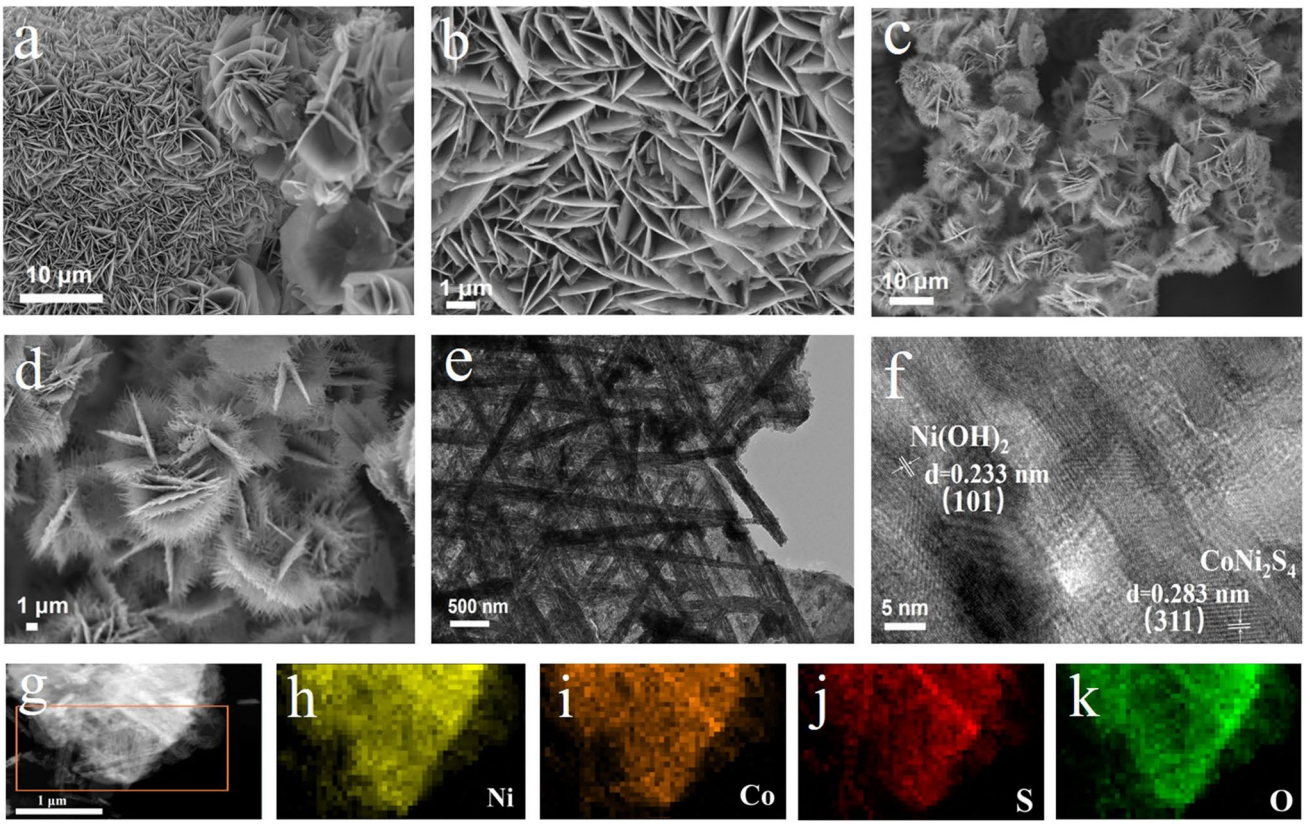

Fig. 3 **a–b** SEM images of $Ni(OH)_2$/NiS/NF, **c–d** SEM images of $Ni(OH)_2/CoNi_2S_4$/NF, **e** TEM image of $Ni(OH)_2/CoNi_2S_4$, **f** HRTEM image of $Ni(OH)_2/CoNi_2S_4$, **g–k** HAADF-STEM image and EDX elemental mappings

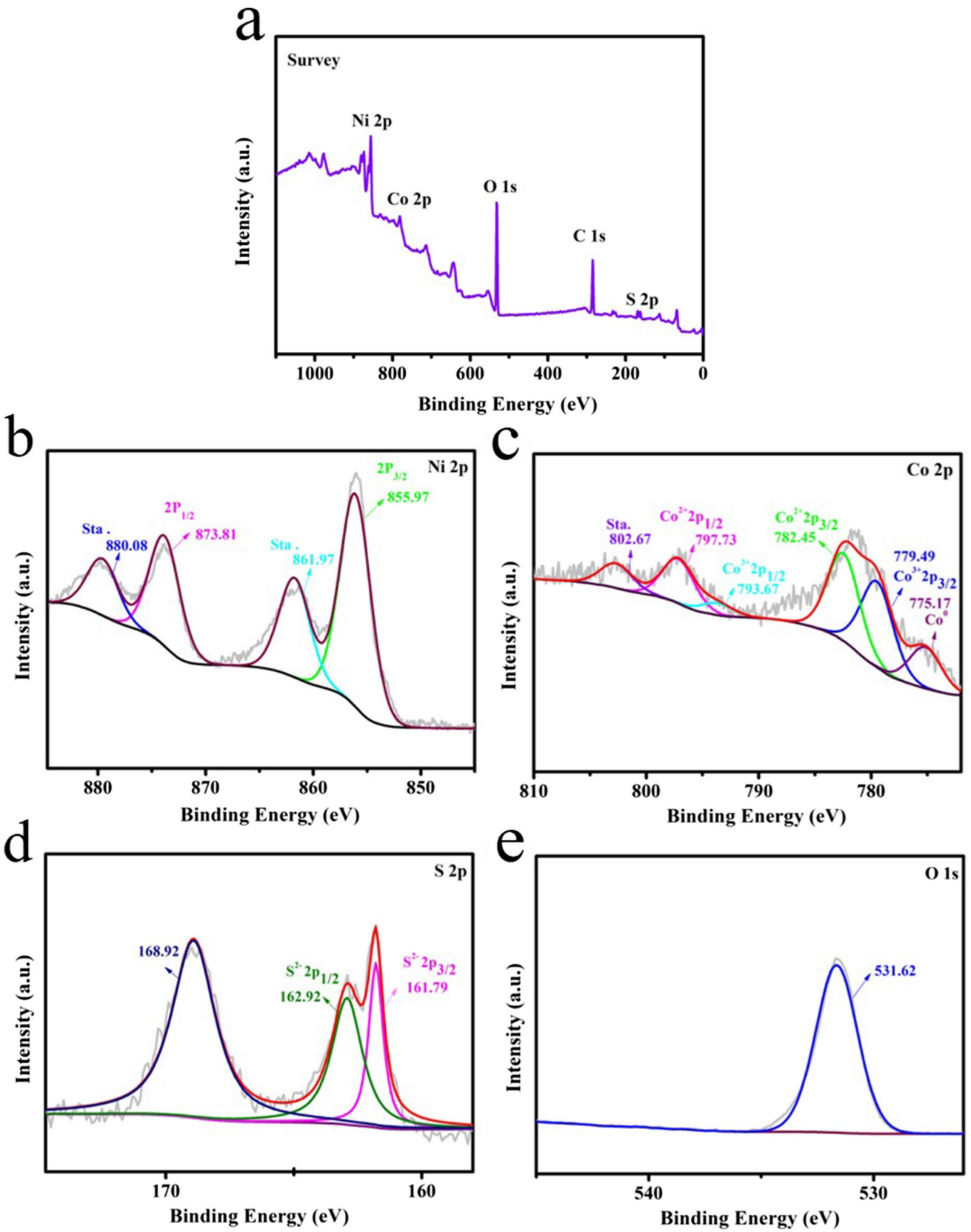

Fig. 4 XPS spectrum of $Ni(OH)_2/CoNi_2S_4$/NF. **a** survey spectrum, **b** Ni 2p, **c** Co 2p, **d** S 2p, and **e** O 1 s

correspond to Co $2p_{3/2}$ and Co $2p_{1/2}$ of Co^{2+} species, and two peaks located at 779.49 and 793.67 eV are ascribed to Co $2p_{3/2}$ and Co $2p_{1/2}$ of Co^{3+} species [40, 42], respectively. The peak at 802.67 eV corresponds to the satellite peak of Co^{2+} species, and the peak appeared at 775.17 eV indicates that there may be Co^0 species in the material [42–44]. As seen from the S 2p spectrum in Fig. 4d, two peaks located at 161.79 and 162.92 eV are ascribed to S $2p_{3/2}$ and S $2p_{1/2}$ of S^{2-} species, respectively. The peak at 168.92 eV may be the sulfur species produced by the surface oxidation of the material exposed in air [34, 45]. The O 1 s spectrum in Fig. 4e displays that the peak located at 531.2 eV are mainly ascribed to OH^- of $Ni(OH)_2$ species [41].

In order to evaluate the electrocatalytic HER performance of $Ni(OH)_2/CoNi_2S_4$/NF, the electrochemical tests were performed in 0.5 M H_2SO_4 using a standard three-electrode cell by LSV at the scanning rate of 5 mV s^{-1}. As shown in Fig. 5a, the overpotential of $Ni(OH)_2/CoNi_2S_4$/NF is only 124 mV at a current density of 10 mA cm^{-2}, which is obviously much lower than that of $Ni(OH)_2$/NiS/NF (229 mV), $Ni(OH)_2$/NF (246 mV), and CoNi LDHs/NF (300 mV). $Ni(OH)_2/CoNi_2S_4$/NF exhibits better HER activity compared with $Ni(OH)_2$/NiS/NF, indicating that the introduction of Co can improve the catalytic activity of the material. Tafel slope is a good indicator of reaction kinetics and the rate-determining step (RDS) of electrocatalytic reactions [46, 47]. As displayed in Fig. 5b, the Tafel slope of $Ni(OH)_2/CoNi_2S_4$/NF is only 84 mV dec^{-1}, indicating that the HER process undergoes Volmer-Heyrovsky mechanism [11]. It is also observed that the $Ni(OH)_2/CoNi_2S_4$/NF shows much smaller Tafel slope than that of $Ni(OH)_2$/NiS/NF (122 mV dec^{-1}), $Ni(OH)_2$/NF (173 mV dec^{-1}), and CoNi LDHs/NF (195 mV dec^{-1}). It demonstrates that $Ni(OH)_2/CoNi_2S_4$/NF has faster electrochemical reaction kinetics, exhibiting better HER catalytic performance. EIS is used to study the electrocatalytic reaction kinetic and the interface characteristics between the electrode and the electrolyte, which reflects the charge-transfer properties. The R_{ct} was calculated by the diameter of the semicircular arc in the Nyquist plots. The smaller the R_{ct} value, the faster the charge-transfer kinetics. Figure 5c presents the Nyquist plots of $Ni(OH)_2/CoNi_2S_4$/NF, $Ni(OH)_2$/NiS/NF, $Ni(OH)_2$/NF, and CoNi LDHs/NF. It can be seen that $Ni(OH)_2/CoNi_2S_4$/NF exhibits the smallest semicircle, demonstrating its lowest R_{ct} value at the electrode/electrolyte interface. The result shows that $Ni(OH)_2/CoNi_2S_4$/NF has stronger charge-transfer ability and faster reaction rate. The electrochemically active surface area (ECSA) reflects the exposure of the active sites, high surface area catalysts can expose more active sites, which can reduce the interaction between catalysts and reactants, which is usually estimated by measuring the C_{dl} at the electrolyte/electrode interface because of their positively proportional correlation ($ECSA = C_{dl}/C_s$) [48, 49]. The C_{dl} values were obtained by performing CV measurements at different scanning rates of 20–100 mV s^{-1} under a non-faradaic potential range in 0.5 M H_2SO_4 (Fig. S4). As displayed in Fig. 5d, $Ni(OH)_2/CoNi_2S_4$/NF exhibits a C_{dl} value of 27 mF cm^{-2}, which is much higher than that of $Ni(OH)_2$/NiS/NF (25 mF cm^{-2}), $Ni(OH)_2$/NF (0.43 mF cm^{-2}), and CoNi LDHs/NF (0.25 mF cm^{-2}). The higher the C_{dl} value of $Ni(OH)_2/CoNi_2S_4$/NF indicates its larger ECSA, which is beneficial to exposing more catalytic active sites and improve the catalytic activity of the material. HER catalysts are required to possess not only good catalytic activity but also good stability. In practical applications, good stability means maintaining good catalytic activity for enough long time. So stability is an important index to evaluate the quality of the catalysts. The cycling stability of $Ni(OH)_2/CoNi_2S_4$/NF was examined by continuous CV with a potential scan from − 0.2 to − 0.8 V at a scan rate of 50 mV s^{-1} for 2000 cycles. From the LSV curves in Fig. 5e, it can be found that $Ni(OH)_2/CoNi_2S_4$/NF displays negligible degradation after 2000 CV cycles. Figure 5f shows the chronopotentiometric curve at a controlled current density of 10 mA cm^{-2} for 30 h. $Ni(OH)_2/CoNi_2S_4$/NF shows a stable potential response for HER without significant degradation after continuous testing for 30 h. The above results reveal that $Ni(OH)_2/CoNi_2S_4$/NF has good catalytic stability in acidic medium.

The above results show that as-synthesized $Ni(OH)_2/CoNi_2S_4$/NF catalyst exhibits better HER catalytic activity and stability. Compared with $Ni(OH)_2$/NiS/NF, the morphology of the catalyst changes from nanosheets to nanoflowers structure composed of nanowire arrays and nanosheets due to the introduction of Co. The unique morphology and structure of $Ni(OH)_2/CoNi_2S_4$/NF is beneficial to increasing the specific surface area and providing more active sites. In situ growth of $Ni(OH)_2/CoNi_2S_4$ on binder-free 3D conductive substrates such as NF can significantly facilitate the conductivity, increase ECSA, promote electron transportation, and improve the catalytic activity of the material. Furthermore, the introduction of Co can improve the electronic structure of the material and produce more active sites. In addition, the synergistic effect of Co and Ni bimetallic sites promotes the HER catalytic activity of the catalyst.

Conclusions

$Ni(OH)_2/CoNi_2S_4$/NF composite was successfully prepared by simple hydrothermal reaction and subsequent sulfurization, used as an efficient electrocatalyst for HER. The results show that as-synthesized $Ni(OH)_2/CoNi_2S_4$/NF catalyst displays better HER catalytic activity and stability in acidic medium. It only requires the low overpotential of 124 mV to drive a current density of 10 mA cm^{-2} with a Tafel slope of 84 mV dec^{-1} in 0.5 M

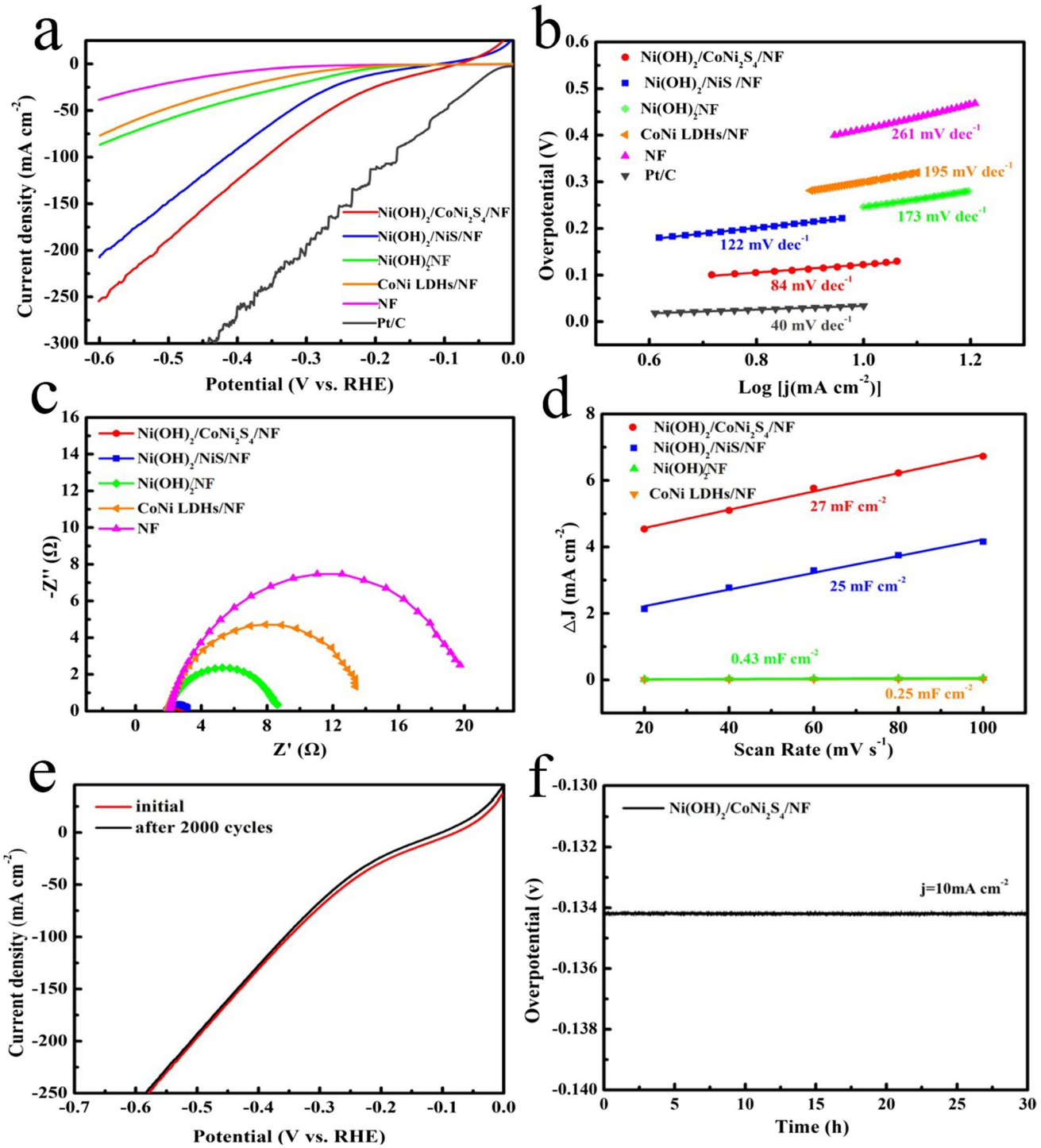

Fig. 5 HER performance of different samples in 0.5 M H_2SO_4 solution. **a** LSV curves, **b** corresponding Tafel slopes, **c** Nyquist plots, **d** electrochemical double-layer capacitance, **e** LSV curves of $Ni(OH)_2/CoNi_2S_4$/NF before and after 2000 CV cycles, **f** chronopotentiometric curve of $Ni(OH)_2/CoNi_2S_4$/NF at a current density of 10 mA cm^{-2} for 30 h

H_2SO_4, exhibiting better catalytic activity than $Ni(OH)_2$/NiS/NF. This is mainly attributed to the unique nanoflowers structure of $Ni(OH)_2/CoNi_2S_4$/NF catalyst, which can increase the active area of the material and provide more catalytic active sites. Meanwhile, the introduction of Co and synergistic effect of Co and Ni bimetallic sites promote the HER activity of the catalyst.

Supplementary Information The online version contains supplementary material available at https://doi.org/10.1007/s11581-022-04824-9.

Acknowledgements This work was supported by the National Natural Science Foundation of China (Grant No. 21865032).

Author contribution Yanxia Wu: conceptualization, methodology, formal analysis, writing (review and editing), project administration. Lirong Su: conceptualization, methodology, formal analysis, investigation, writing-original draft, writing—review and editing. Qingtao Wang: super-vision, writing—review and editing. Shufang Ren: supervision, writing—review and editing.

Declarations

Conflicts of interest The authors declare no competing interests.

References

1. Zhang JY, Wang H, Tian Y, Yan Y, Xue Q, He T, Liu H, Wang C, Chen Y, Xia BY (2018) Anodic hydrazine oxidation assists energy efficient hydrogen evolution over a bifunctional cobalt perselenide nanosheet electrode. Angew Chem Int Ed 57:7649–7653
2. Mahmood N, Yao Y, Zhang JW, Pan L, Zhang X, Zou JJ (2018) Electrocatalysts for hydrogen evolution in alkaline electrolytes: mechanisms, challenges, and prospective solutions. Adv Sci 5:1700464
3. Hu Q, Han Z, Wang X, Li G, Wang Z, Huang X, Yang H, Ren X, Zhang Q, Liu J, He C (2020) Facile synthesis of sub-nanometric copper clusters by double confinement enables selective reduction of carbon dioxide to methane. Angew Chem Int Ed 59:19054–19059
4. Gao M, Chen L, Zhang Z, Sun X, Zhang S (2018) Interface engineering of the $Ni(OH)_2$-Ni_3N nanoarray heterostructure for the alkaline hydrogen evolution reaction. J Mater Chem A 6:833–836
5. Upadhyay S, Pandey OP (2022) Synthesis of Mo_2C/MoC/C nanocomposite for hydrogen evolution reaction. J Solid State Electr 26:559–564
6. Jiang M, Zou Y, Xu F, Sun L, Hu Z, Yu S, Zhang J, Xiang C (2022) Synthesis of g-C_3N_4/Fe_3O_4/MoS_2 composites for efficient hydrogen evolution reaction. J Alloy Compd 906:164265
7. Liu X, Ni K, Wen B, Guo R, Niu C, Meng J, Li Q, Wu P, Zhu Y, Wu X, Mai L (2019) Deep reconstruction of nickel-based precatalysts for water oxidation catalysis. ACS Mater Lett 4:2585–2592
8. Pei Y, Ge Y, Chu H, Smith W, Dong P, Ajayan PM, Ye M, Shen J (2019) Controlled synthesis of 3D porous structured cobalt-iron based nanosheets by electrodeposition as asymmetric electrodes for ultra-efficient water splitting. Appl Catal B 244:583–593
9. Ma M, Zheng Z, Song Z, Zhang X, Han X, Chen H, Xie Z, Kuang Q, Zheng L (2020) In situ construction and post-electrolysis structural study of porous Ni_2P@C nanosheet arrays for efficient water splitting. Inorg Chem Front 7:2960–2968
10. Ye S, Luo F, Zhang Q, Zhang P, Xu T, Wang Q, He D, Guo L, Zhang Y, He C, Ou YX, Gu M, Liu J, Sun X (2019) Highly stable single Pt atomic sites anchored on aniline-stacked graphene for hydrogen evolution reaction. Energy Environ Sci 12:1000–1007
11. Xie L, Wang L, Zhao W, Liu S, Huang W, Zhao Q (2021) WS_2 moiré superlattices derived from mechanical flexibility for hydrogen evolution reaction. Nat Commun 12:1–9
12. Chen J, Tang Y, Wang S, Xie L, Chang C, Cheng X, Liu M, Wang L, Wang L (2022) Ingeniously designed Ni-Mo-S/$ZnIn_2S_4$ composite for multi-photocatalytic reaction systems. Chinese Chem Lett 33:1468–1474
13. Fan K, Chen H, Ji Y, Huang H, Claesson PM, Daniel Q, Philippe B, Rensmo H, Li F, Luo Y, Sun L (2016) Nickel-vanadium monolayer double hydroxide for efficient electrochemical water oxidation. Nat Commun 7:1–9
14. Wu Z, Zou Z, Huang J, Gao F (2018) Fe-doped NiO mesoporous nanosheets array for highly efficient overall water splitting. J Catal 358:243–252
15. Gao D, Guo J, He H, Xiao P, Zhang Y (2022) Geometric and electronic modulation of fcc NiCo alloy by Group-VI B metal doping to accelerate hydrogen evolution reaction in acidic and alkaline media. Chem Eng J 430:133110
16. Peng C, Li T, Zou Y, Xiang C, Xu F, Zhang J, Sun L (2021) Bacterial cellulose derived carbon as a support for catalytically active Co-B alloy for hydrolysis of sodium borohydride. Int J Hydrogen Energy 46:666–675
17. Wei Z, Hu X, Ning S, Kang X, Chen S (2019) Supported heterostructured MoC/Mo_2C nanoribbons and nanoflowers as highly active electrocatalysts for hydrogen evolution reaction. ACS Sustain Chem Eng 7:8458–8465
18. Wan J, Wu J, Gao X, Li T, Hu Z, Yu H, Huang L (2017) Structure confined porous Mo_2C for efficient hydrogen evolution. Adv Funct Mater 27:1703933
19. Zhang J, Xiao W, Xi P, Xi S, Du Y, Gao D, Ding J (2017) Activating and optimizing activity of CoS_2 for hydrogen evolution reaction through the synergic effect of N dopants and S vacancies. ACS Energy Lett 2:1022–1028
20. Yan L, Cao L, Dai P, Gu X, Liu D, Li L, Wang Y, Zhao X (2017) Metal-organic frameworks derived nanotube of nickel-cobalt bimetal phosphides as highly efficient electrocatalysts for overall water splitting. Adv Funct Mater 27:1703455
21. Li H, Chen S, Zhang Y, Zhang Q, Jia X, Zhang Q, Gu L, Sun X, Song L, Wang X (2018) Systematic design of superaerophobic nanotube-array electrode comprised of transition-metal sulfides for overall water splitting. Nat Commun 9:1–12
22. Wang R, Liu B, You S, Li Y, Zhang Y, Wang D, Tang B, Sun Y, Zou J (2022) Three-dimensional Ni_3Se_4 flowers integrated with ultrathin carbon layer with strong electronic interactions for boosting oxygen reduction/evolution reactions. Chem Eng J 430:132720
23. Chen LX, Chen ZW, Wang Y, Yang CC, Jiang Q (2018) Design of dual-modified MoS_2 with nanoporous Ni and graphene as efficient catalysts for the hydrogen evolution reaction. ACS Catal 8:8107–8114
24. Xue Y, Zuo Z, Li Y, Liu H, Li Y (2017) Graphdiyne-supported $NiCo_2S_4$ nanowires: a highly active and stable 3D bifunctional electrode material. Small 13:1700936
25. Kim JY, Han S, Bang JH (2017) Cobalt disulfide nano-pine-tree array as a platinum alternative electrocatalyst for hydrogen evolution reaction. Mater Lett 189:97–100
26. Zeleke TS, Tsai MC, Weret MA, Huang CJ, Birhanu MK, Liu TC, Huang CP, Soo YL, Yang YW, Su WN, Hwang BJ (2019) Immobilized single molecular molybdenum disulfide on carbonized polyacrylonitrile for hydrogen evolution reaction. ACS Nano 13:6720–6729
27. Lin J, Wang P, Wang H, Li C, Si X, Qi J, Cao J, Zhong Z, Fei W, Feng J (2019) Defect-rich heterogeneous MoS_2/NiS_2 nanosheets electrocatalysts for efficient overall water splitting. Adv Sci 6:1900246
28. Wu L, Xu X, Zhao Y, Zhang K, Sun Y, Wang T, Wang Y, Zhong W, Du Y (2017) Mn doped MoS_2/reduced graphene oxide hybrid for enhanced hydrogen evolution. Appl Surf Sci 425:470–477
29. Zhang R, Zhu Z, Lin J, Zhang K, Li N, Zhao C (2020) Hydrolysis assisted in-situ growth of 3D hierarchical FeS/NiS/nickel foam electrode for overall water splitting. Electrochim Acta 332:135534
30. Wang P, Qi J, Li C, Li W, Wang T, Liang C (2020) Hierarchical $CoNi_2S_4$@NiMn-layered double hydroxide heterostructure

nanoarrays on superhydrophilic carbon cloth for enhanced overall water splitting. Electrochim Acta 345:136247
31. Zhang X, Lai Z, Ma Q, Zhang H (2018) Novel structured transition metal dichalcogenide nanosheets. Chem Soc Rev 47:3301–3338
32. Shi E, Gao Y, Finkenauer BP, Coffey AH, Dou L (2018) Two-dimensional halide perovskite nanomaterials and heterostructures. Chem Soc Rev 47:6046–6072
33. Ding Y, Du X, Zhang X (2022) Rose-like Cu-doped Ni_3S_2 nanoflowers decorated with thin NiFe LDH nanosheets for high-efficiency overall water and urea electrolysis. Appl Surf Sci 584:152622
34. Wu F, Guo X, Hao G, Hu Y, Jiang W (2019) Self-supported hollow $Co(OH)_2$/NiCo sulfide hybrid nanotube arrays as efficient electrocatalysts for overall water splitting. J Solid State Electr 23:2627–2637
35. Peng O, Shi R, Wang J, Zhang X, Miao J, Zhang L, Fu Y, Madhusudan P, Liu K, Amini A, Cheng C (2020) Hierarchical heterostructured nickle foam-supported Co_3S_4 nanorod arrays embellished with edge-exposed MoS_2 nanoflakes for enhanced alkaline hydrogen evolution reaction. Mater Today Energy 18:100513
36. Duan JJ, Han Z, Zhang RL, Feng JJ, Zhang L, Zhang QL, Wang AJ (2021) Iron, manganese co-doped Ni_3S_2 nanoflowers in situ assembled by ultrathin nanosheets as a robust electrocatalyst for oxygen evolution reaction. J Colloid Interf Sci 588:248–256
37. Chen MT, Duan JJ, Feng JJ, Mei LP, Jiao Y, Zhang L, Wang AJ (2022) Iron, rhodium-codoped Ni_2P nanosheets arrays supported on nickel foam as an efficient bifunctional electrocatalyst for overall water splitting. J Colloid Interf Sci 605:888–896
38. Du X, Yang Z, Li Y, Gong Y, Zhao M (2018) Controlled synthesis of $Ni(OH)_2/Ni_3S_2$ hybrid nanosheet arrays as highly active and stable electrocatalysts for water splitting. J Mater Chem A 6:6938–6946
39. Zhang RL, Feng JJ, Yao YQ, Fang KM, Zhang L, Yin ZZ, Wang AJ (2021) Straw-like phosphorus-doped Co_2MnO_4 nanoneedle arrays supported on nickel foam for high-efficiency hydrogen evolution reaction in wide pH range of electrolytes. Appl Surf Sci 548:149280
40. Su C, Xu S, Zhang L, Chen X, Guan G, Hu N, Su Y, Zhou Z, Wei H, Yang Z, Qin Y (2019) Hierarchical $CoNi_2S_4$ nanosheet/nanotube array structure on carbon fiber cloth for high-performance hybrid supercapacitors. Electrochim Acta 305:81–89
41. Liu Y, Wang J, Tian Q, Liu M, Wang X, Li P, Li W, Cai N, Chen W, Yu F (2019) Papillae-like morphology of $Ni/Ni(OH)_2$ hybrid crystals by stepwise electrodeposition for synergistically improved HER. CrystEngComm 21:3431–3438
42. Dai W, Ren K, Zhu YA, Pan Y, Yu J, Lu T (2020) Flower-like $CoNi_2S_4/Ni_3S_2$ nanosheet clusters on nickel foam as bifunctional electrocatalyst for overall water splitting. J Alloy Compd 844:156252
43. Sivanantham A, Ganesan P, Shanmugam S (2016) Hierarchical $NiCo_2S_4$ nanowire arrays supported on Ni foam: an efficient and durable bifunctional electrocatalyst for oxygen and hydrogen evolution reactions. Adv Funct Mater 26:4661–4672
44. Mai W, Cui Q, Zhang Z, Zhang K, Li G, Tian L, Hu W (2020) CoMoP/NiFe-layered double-hydroxide hierarchical nanosheet arrays standing on Ni foam for efficient overall water splitting. ACS Appl Energy Mater 3:8075–8085
45. Yang Y, Yao H, Yu Z, Islam SM, He H, Yuan M, Yue Y, Xu K, Hao W, Sun G, Li H, Ma S, Zapol P, Kanatzidis MG (2019) Hierarchical nanoassembly of $MoS_2/Co_9S_8/Ni_3S_2/Ni$ as a highly efficient electrocatalyst for overall water splitting in a wide pH range. J Am Chem Soc 141:10417–10430
46. Hu Q, Gao K, Wang X, Zheng H, Cao J, Mi L, Huo Q, Yang H, Liu J, He C (2022) Subnanometric Ru clusters with upshifted D band center improve performance for alkaline hydrogen evolution reaction. Nat commun 13:1–10
47. Cheng Z, Wang X, Yang H, Yu X, Lin Q, Hu Q, He C (2021) Construction of cobalt-copper bimetallic oxide heterogeneous nanotubes for high-efficient and low-overpotential electrochemical CO_2 reduction. J Energy Chem 54:1–6
48. Zhang W, Chen YP, Zhang L, Feng JJ, Li XS, Wang AJ (2022) Theophylline-regulated pyrolysis synthesis of nitrogen-doped carbon nanotubes with iron-cobalt nanoparticles for greatly boosting oxygen reduction reaction. J Colloid Interf Sci 626:653–661
49. Chen MT, Zhang RL, Feng JJ, Mei LP, Jiao Y, Zhang L, Wang AJ (2022) A facile one-pot room-temperature growth of self-supported ultrathin rhodium-iridium nanosheets as high-efficiency electrocatalysts for hydrogen evolution reaction. J Colloid Interf Sci 606:1707–1714